Dense metallic hydrogen sulfide-ammonia ices

Xiaofeng Li[†, ‡], Angus Lowe[‡], Lewis Conway[‡], Maosheng Miao[§, #], Andreas Hermann[‡, *]

[†]College of Physics and Electronic Information, Luoyang Normal University, Luoyang 471934, P. R. China

[‡]Centre for Science at Extreme Conditions and SUPA, School of Physics and Astronomy, The University of Edinburgh, Edinburgh EH9 3FD, United Kingdom

[§]Department of Chemistry & Biochemistry, California State University, Northridge, CA, 91330-8262, USA.

[#] Beijing Computational Science Research Center, Beijing, 100193, China

Hydrogen sulfide (H_2S) and ammonia (NH_3) form hydrogen-bonded molecular mixtures at ambient conditions, but their phase behavior and propensity towards mixing under pressure is not well understood. Such mixtures dominate the interiors of icy planets and open up new routes towards hydrogen-rich superconductors. Here we report on stable phases in the H_2S-NH_3 system under extreme pressure conditions to 4 Mbar from first-principles crystal structure prediction methods. We identify four stable compositions, two of which, (H_2S) (NH_3) and (H_2S) (NH_3)$_4$, are stable in a sequence of structures to the Mbar regime. A re-entrant stabilization of (H_2S) (NH_3)$_4$ above 300GPa is driven by a marked reversal of sulfur-hydrogen chemistry. Several stable phases exhibit metallic character, which enables superconductivity. Electron-phonon coupling calculations predict superconducting temperatures up to 50K, in the *Cmma* phase of (H_2S) (NH_3) at 150GPa. The present findings suggest a reservoir for hydrogen sulfide in the upper mantle regions of icy planets in a potentially metallic mixture, which has implications for their magnetic field formation. They also shed light on potential routes towards superconducting H_2S-containing molecular mixtures.

The icy giants of our solar system, below gaseous atmospheres dominated by hydrogen and helium, are thought to contain thick "hot ice" layers consisting of a mixture dominated by water, methane and ammonia at extreme pressure-temperature conditions that reach several Mbar and several thousand Kelvin[1-3]. Unlike the Jovian planets, which are dominated throughout by hydrogen/helium, complex chemical processes are expected for "hot ice" mixtures of molecular fluids at deep planetary conditions [4,5], including losing their original molecular nature, the formation of exotic states such as "superionic" water or ammonia, potential demixing, and so on [6, 7]. The physical and chemical properties of the "hot ice" layers will greatly influence the gravitational moments, rotational velocities and atmospheric composition as well as the thermal evolution and internal structure of these celestial bodies. However, relatively little information is available to unambiguously explain the interior structure and composition of planet such as Uranus and Neptune, let alone the large set of icy or water planets discovered outside our solar system[8-10]. Realistic studies of the "hot ice" mixtures are therefore paramount to expand our understanding of these planetary environments. High-pressure experiments, e.g. on "synthetic Uranus", hydrocarbons, and binary molecular mixtures have shown diverse chemistry and unexpected reactivity under specific pressure-temperature conditions[11-13]. Meanwhile, electronic structure calculations have studied various mixtures of molecular ices and their interactions with the lighter atmosphere constituents hydrogen and helium and predict a plethora of stable compounds and exotic states of matter, such as plasticity and staged superionicity[14-21].

One molecular component that has received little attention in this area is hydrogen sulfide, H_2S. Its high-pressure properties have of course been of tremendous interest recently, due to the conventional superconductivity found in H_2S above 200K at pressures around 155GPa [22-27]. But it also plays a role in a planetary context, as atmospheric observations in Uranus and Neptune reveal the existence of substantial amount of H_2S in those planets [28-30]. Recent predictions of a superconducting metastable H_3S-methane compound highlight the overlap between planetary science and materials science aspects when studying dense molecular mixtures [31,32] and a carbonaceous sulfur hydride compound has been reported as the first room-temperature superconductor[33]. However, the structure of the superconducting material is unknown. To develop a detailed understanding of what drives the superconductivity, with the ultimate aim of reducing the pressures required to generate the superconducting state, systematic investigations of the

interaction of H_2S with molecular species at high pressures are needed, but these are mostly missing.

An alternative molecular compound that should react with H_2S is ammonia, NH_3. In a planetary context, this mixture is highly relevant. It is presumed that H_2S and NH_3 form ammonium hydrosulfide (NH_4SH) and ammonium sulfide ($(NH_4)_2S$) clouds in the lower atmospheres of Uranus, Neptune, and the Jovian planets[34,35]. However, the atmospheric abundances of nitrogen and sulfur inferred from microwave absorption experiments are heavily distorted from solar ratios, and constraints of interior S/N and N/H ratios are complicated by possible sequestration of H_2S or NH_3 deeper inside the planets' icy oceans [35-38]. NH_4SH has been known since the 19th century [39] and its crystal structure and infrared (IR) and optical absorption properties have been studied extensively[40-44]. These studies do not address the potential formation of high-pressure compounds of H_2S and NH_3, which could form a reservoir deep inside the planets' mantle regions. Recent studies of the analogue water-ammonia system showed a propensity towards the formation of ionic compounds at high pressure, stabilized in part by full disintegration of the water molecule[15,45,46]. If the analogy to ammonia-water mixtures holds for compressed H_2S-NH_3, one may expect novel compositions under pressure and formation of ionic compounds, but in addition potentially also metallic phases. Conducting "hot ice" phases are thought to cause the non-dipolar magnetic fields of Uranus and Neptune[47, 48].

There are therefore multiple motivations to study molecular mixtures that include H_2S at extreme conditions: (i) Can the observation of hydrogen sulfide in icy planets' atmospheres be explained by a reservoir of bound compounds at elevated pressures? (ii) Can analogies be drawn to the behavior of hydrogen sulfide's homologue, water, with its predicted de-protonated ionic phases in mixtures with ammonia? (iii) Does the pressure-induced metallization and superconductivity of H_2S and H_2S-CH_4 mixtures translate to other relevant molecular mixtures? Studying mixtures of H_2S and NH_3 under compression not only has important significance for understanding planetary interiors but also for the physics of hydrogen-bonded molecular compounds in general and for materials science.

To explore these questions, we study here the potential formation of hydrogen sulfide-ammonia mixtures under high-pressure conditions up to 800GPa using ab-initio calculations, and present a theoretical overview of their phase diagrams, including stable metallic

and superconducting phases with novel bonding configurations, driven by a reversal of sulfur chemistry from an electronegative isolated S^{2-} anion to an electropositive S^{6+} polyhedra-former.

Results

Stable Compounds and Structures. To find the stable H_2S-NH_3 compounds, we performed extensive structure searches on various compositions of $(H_2S)_x$ $(NH_3)_y$ under pressure. Fig.1 (a) exhibits the resulting convex hulls of the binary compounds of H_2S-NH_3 below 60GPa. At zero pressure, three stable compounds AMS, ADS, and AHS are stable against decomposition into NH_3 and H_2S. ADS and AHS decompose into AMS+ammonia at 5GPa (Fig.S5 in the Supplementary Information) and AMS+ADS at 3GPa (Fig.S6), respectively. When pressure increases above 2GPa, a new compound AQS becomes stable (Fig.S7). The convex hull above 60GPa (relative to ammonia, H_3S and S) is shown in Fig.1 (b, c). AQS remains stable up to 83GPa, when it decomposes into AMS+H_3S+S. AMS remains stable up to 129GPa (Fig.S8) before decomposing into the constituent ices NH_3, H_3S and S. Among all compounds, AMS is the most thermodynamically stable mixture throughout the low pressure range, i.e. has the largest formation enthalpy per molecule. What is particularly interesting is the re-entrant stability of AQS above 300GPa (Fig. 1 (c), Fig.S7), which is due to intriguing changes in chemistry we will examine later. We did not find any stable phases for ATS at any pressure conditions but Figs. S9-S12 and Tables S5-S6 list the properties of the most relevant metastable phases.

The ground state stability ranges for all compounds are summarized in the phase diagram Fig. 1(d), which also depicts all structure changes as function of pressure. At ambient conditions, we successfully reproduce the low-pressure tetragonal P4/nmm phase of AMS [Fig.S8] as reported by Bragin et.al.[40]; this is the same structure adopted by AMH (NH_3:H_2O) at pressures above 10GPa [15]. We find that AMS should transform from P4/nmm to a monoclinic Cc phase and further to a $P2_1/m$ phase at 11GPa and 50GPa respectively, followed by orthorhombic Abm2 at 94GPa and Cmma at 125GPa. The low pressure P4/nmm and Cc phases, shown in Fig.2 (a, b), form simple ionic $(NH_4)^+(SH)^-$ arrangements; they differ in the layout of the S-H⋯S-H hydrogen bonded chains, which are linear in P4/nmm and kinked in Cc. $P2_1/m$ [Fig.2 (c)] represents an evolution of the Cc phase, in which $(SH)^-$ anions form hydrogen-bonded 1D chains with linear symmetric S-H-S bonds; the pressure for hydrogen bond symmetrization (50 GPa) is consistent with that seen

in other ices and minerals [49,50]. At higher pressure, the orthorhombic phase Abm2 [Fig.2 (d)] returns to the ionic $(NH_4)^+(SH)^-$ motif while Cmma [Fig.2 (e)] has kinked infinite –(H-S)- chains with symmetric buckled S-H-S bonds in a matrix of NH_4^+ cations; structural motifs seen for instance throughout the alkali hydroxides $M^+(OH^-)$ [51].

For ammonium sulfide, $(NH_4)_2S$, here labelled AHS, we find a high-symmetry Fm-3m phase [Fig.2 (f)] as the stable ground state at zero pressure. It is an anti-fluorite structure with NH_4^+ cations on the fluorine sites, which are hydrogen-bonded to adjacent S^{2-} anions. Significantly, two further compounds were also uncovered as stable at zero pressure - ADS (in a monoclinic phase $P2_1/m$) [Fig.2 (g)] and AQS (in a sequence of structures) [Fig.2 (h-j)]. $P2_1/m$-ADS is characterized as $(NH_4)^+(HS)^-(H_2S)$. The (HSH)···(SH) sublattice forms a hydrogen-bonded network. However, both AHS and ADS quickly become unstable under pressure.

In contrast, AQS emerges as a very stable mixture, firstly with a $P2_1/m$ phase [Fig.2 (h)] that has S^{2-} anions surrounded by $(NH_4)^+$ and NH_3. It converts to a higher-symmetry tetragonal I4/m phase [Fig.2 (i)] at 58GPa. The tetragonal phase features S^{2-} anions and the unusual $(N_2H_7)^+$ cation, which was also reported in AQH ($(NH_3)_4(H_2O)$) [15] and is known from ammonium iodide salts [52]. AQS then decomposes into AMS and S at 83GPa (Fig.S7). However, when pressure is increased up to 300GPa, a re-stabilized mixture in a monoclinic P-1 phase [Fig.2 (j)] should be recovered from NH_3, H_3S and S. This re-emergent phase remains stable up to 525GPa. The chemical bonding in this high-pressure phase is completely different from the low-pressure polymorphs of AQS. The $(N_2H_7)^+$ cation is replaced by ammonium, $(NH_4)^+$; the S^{2-} anion is replaced by a $(HN\text{-}(SH_4)\text{-}NH)^{2-}$ cluster, with a central S atom that is connected to four H atoms and two (NH) groups.

Equation-of-state. Previous calculations on ammonia hydrates suggested that ammonia-rich hydrate could precipitate out of any ammonia-water mixture and form a layer above a water-rich ocean [45]. Our equation-of-state calculations (Fig.S13) suggest that the AMS compound would be situated between those layers; for instance, at 80 GPa, AMS has a gravimetric density of 2.79 g/cm^3, which is heavier than ammonia hemihydrate (2.44 g/cm^3) and lighter than ice VIII/X (2.99 g/cm^3). This suggests hydrogen sulfide could be bound in stable ionic compounds with ammonia in reservoirs towards the top of the “hot ice” mantle regions.

Discussion

Chemical Bonding. At low pressures, below around 1Mbar, the hydrogen sulfide-ammonia mixtures adhere to the expected chemical picture: H_2S molecules are likely to disintegrate, with protons transferring to NH_3 molecules as much as possible. As a consequence, ionic structures form (with isolated S^{2-} anions in ammonia-rich phases) that are further stabilized by hydrogen bonding. These interpretations are supported by topological analyses of the electronic charge density using the Bader QTAIM approach, and the ELF. Figures S14-S16 and Tables S6-S8 show the ELF and Bader partial charges, respectively, for the structures discussed so far. Partial charges of isolated sulfur atoms (from -0.89 to -1.23 in AHS and AQS) are consistent with a formal oxidation state -2.

However, at high pressures, and led by the re-emergence of stable AQS, an interesting reversal of chemistry occurs. Sulfur changes from an isolated anion to instead form the central atom of different octahedral clusters. In P-1-AQS, sulfur forms $[SH_4(NH)_2]^{2-}$ clusters that are packed together with NH_4^+ cations. In both AHS and AMS at high pressures, the most stable phases (though metastable against decomposition) feature sulfur at the centers of -(SH_4N_2)- and -(SH_2N_2)- clusters, respectively (see Fig.S15-S17). Only in ADS, the most H_2S-rich compound studied here, did we not find such a role reversal for sulfur. The QTAIM analysis (see Tables S6-S8) confirms the drastic changes in the character of sulfur and hydrogen. For AQS-$P2_1/m$ at 20GPa and AQS-I4/m at 70GPa, every hydrogen donates about 0.43e; both N and S act as electron acceptors, with partial charges of -1.21e (-1.22e) and -1.12e (-1.01e), respectively. When pressure increases up to 400GPa, in AQS-P-1, S instead *donates* 2.45e while the terminal H atoms *accept* about 0.26e in the formation of $(HN)^{2-}$-$(SH_4)^{2+}$-$(NH)^{2-}$. There are two types of N atoms in NH^{2-} and NH_4^+ groups, which accept about 1.64e and 1.27e, respectively. Sulfur and hydrogen atoms demonstrate an extraordinary capacity to switch between electron donor and acceptor, and vice versa. The same reversal in charge transfer can be seen in solid H_3S itself (see Fig. S19), albeit on a much smaller numerical scale: in the low-pressure molecular Cccm and R3m phases of H_3S, sulfur is a weak electron acceptor, but within the atomic (and most relevant superconducting) Im-3m phase it eventually (at 400GPa) transforms into a weak electron donor.

To further characterize the nature of the bonding in the mixtures, we calculated the COHP and integrated COHP (ICOHP) for AQS-I4/m at 70GPa and AQS-P-1 at 400GPa. A *negative*

COHP below the Fermi level indicates bonding states, whereas *positive* COHP indicates antibonding states. Fig. 3 shows the average COHP and ICOHP of nearest-neighbour N-H, S-H and S-N interactions for both AQS phases. In both structures covalent N—H bonding is most prominent (Fig. 3(a) also reveals partially occupied anti-bonding states in the N_2H_7 units). In contrast, see Fig. 3(a), both S-H and S-N bonding is very weak – consistent with having isolated S^{2-} anions hydrogen-bonded to N_2H_7. In the P-1 phase, S-H (S-N) bonds between the nearest neighboring S-H (S-N) pairs also have smaller COHP values than N-H (Fig. 3(b)), indicating weaker covalent bonding, but are much larger than in the I4/m phase: the average ICOHP for each S-H and S-N bond is -2.1 in the P-1 phase, compared to -1.17 and -0.53 in I4/m. Furthermore, the nearest S–H (1.84 Å) and S–N (2.82 Å) distances in I4/m phase at 70GPa are both much larger than in the P-1 phase (1.28 and 1.52 Å, respectively); this compares to covalent S–H and S–N bond lengths of 1.59 Å in H_3S at 40GPa[21] and 1.70 Å in solid N_4S_4 at ambient pressure[53]. By comparison, the S-H bonding in pure H_3S is relatively weak (Fig. S19, ICOHP = -0.5 at 400 GPa), which illustrates how the ad-mixture of NH_3 can improve the bonding strengths of H-S or N-S atoms greatly.

Finally, to further illuminate why pressure is able to induce those changes, we examined the evolution of the contributions to the formation enthalpy $H = U + PV$, the internal energy (U) and the product of pressure and volume (PV), for the stable AQS phases in response to pressure change. In Fig.4(a), the pressure dependence of ΔU, $\Delta(PV)$, and ΔH for the $P2_1/m$ and I4/m phases are shown relative to the reference decomposition $4*NH_3+(2H_3S+S)/3$. Both compounds are stabilized by internal energy against decomposition (likely due to ionic bonding), whereas the $\Delta(PV)$ term is positive for both. I4/m-AQS is more compact, which leads to the phase transition from $P2_1/m$ to I4/m at 58GPa. Above 58GPa, the ΔU and $\Delta(PV)$ terms for I4/m are relatively well balanced, resulting ultimately in decomposition of AQS at 91GPa into NH_3, H_3S and S. For the high pressure P-1-AQS phase (Fig.4(b)) the picture has reversed: the $\Delta(PV)$ is strongly negative while ΔU is positive. The re-emergence of AQS at 300GPa is due to its more compact structure that centers around the small S cation, which outweighs the electronic cost of ionizing the sulfur 3p-shell.

Electronic Properties. Molecular “hot ice” mixtures are usually electronically not very interesting wide gap insulators and require very extreme conditions to close the band gaps.

However, H_2S and H_3S metallize at relatively low pressures, below 1 Mbar. This property seems to translate to their mixtures with methane, CH_4, ultimately resulting in a room temperature superconducting material at 250 GPa[31]. Therefore, the electronic structures of all the stable mixtures found here were calculated within their stability ranges, and partial densities of states (DOS) compiled in Fig. S20-S23. These show that ADS, AHS and AQS all retain wide band gaps below 100GPa. For AMS, the P4/nmm, Cc and $P2_1/m$ phases all have wide band gaps below 90GPa. At higher pressure we observe that Abm2-AMS and Cmma-AMS (Fig.S21 (d, e)) exhibit metallic character. In our calculations Abm2-AMS experiences band gap closure from semiconductor to metal at about 88GPa (Fig.S21 (i)), possibly underestimated at DFT-PBE level of theory, and at the upper end of its range of stability. The Cmma-AMS phase is metallic in its full range of stability. To find metallic molecular mixtures at these relatively low pressures remains unusual. A metallic fluid of H_2-H_2O was predicted above 5000K and 500 GPa [20] while hot dense hydrogen seems to require at least 1500K at 150 GPa [54, 55]. On the other hand, H_2S itself metallizes at 96 GPa [56,57], an unknown carbonaceous H_2S material was reported to metallize at 60 GPa [33], and metastable CH_4-H_2S mixtures were predicted to be metallic at 100 GPa and above [31, 32]. Here, we find that specific stable mixtures of H_2S with ammonia retain this property.

The Fermi energies for the Abm2 phase at 100GPa and Cmma phase at 200GPa (Fig.S21 (d, e)) are located at shoulders of a valence peaks in the DOS that dominated by N-2p and S-3p states, leading to non-negligible values of the DOS at E_f in particular for Cmma-AMS. These features are potentially favorable for high-temperature superconductivity. We therefore calculated the electron-phonon coupling to investigate the superconductivity of these high-pressure phases of AMS. Fig.5 (a, b) shows the projected phonon density of states (PHDOS), Eliashberg spectral function $\alpha^2F(\omega)$, and electron-phonon coupling integral $\lambda(\omega)$ for Abm2- and Cmma-AMS under pressure. A notable feature of phonon density of states for both phases is the separation of the vibrational modes into three distinct regions: The lower frequencies (below 20 THz) are associated with lattice modes of the heavier S and N atoms, and some of hydrogen atoms; the intermediate frequencies (between 20 and 60THz) are mainly derived from combinations of molecular libration, bending, and stretching modes; and the highest frequencies (80~100 THz) are derived primarily from the N-H stretching modes of the molecular NH_4 units. The contribution to $\lambda(\omega)$ is mainly from the low frequency (0-20 THz, about 56.8%) and mid-frequency region (20-60THz, about

34.1%), while the highest vibrons (80~100 THz) contribute about 9.1%. The superconducting temperatures are estimated by the Allen-Dynes modified McMillan equation[58], using typical value (μ^*=0.1) of the Coulomb pseudopotential. The calculated values of λ, ω_{log} and T_c of the Abm2 and Cmma phases of AMS under pressure are shown in Table 1. The Cmma-AMS phase at 150GPa has the largest λ value of 0.995 and with ω_{log}=697K, leads to a T_c of 49.9K. This represents the largest T_c found here, as further compression results in a decrease of T_c. Table S10 lists predicted T_c values for other, metastable, phases, which can also reach up to 46K (in ADS at 300 GPa).

Conclusions

In summary, we performed an extensive structure search in combination with first-principles total energy calculations to explore the formation, stability, chemical bonding and electronic properties of hydrogen sulfide-ammonia ices at high pressure. While only two mixed compounds, NH_4SH and $(NH_4)_2S$, are known to exist at or near ambient conditions (and we confirm their stability) we report a series of new phases across four different stoichiometries (ADH, AMS, AHS, and AQS) with very different high-pressure properties. Two compounds, ADS and AHS, are stable only at very low pressures, while AMS is stable at moderate pressure in a series of different phases up to 129GPa. AQS is initially stable at pressures below 83GPa. However, it becomes stable again under higher pressure above 300GPa and remains such up to 525GPa through an interesting reversal of the sulfur chemistry.

At low pressures, the H_2S species in these compounds disintegrates very rapidly, with the sequence $H_2S \rightarrow (HS)^- \rightarrow S^{2-}$ that can be triggered as low as ambient pressure; accordingly, the compounds feature NH_3, NH_4^+, and $N_2H_7^+$ species, depending on stoichiometry. The ionic bonding helps to stabilize these structures and all elements are, corroborated by QTAIM analysis, in expected oxidation states (S^{2-}, N^{3-}, and H^+) that correlate with their electronegativities (Pauling scale: 2.58/3.04/2.20 for S/N/H). At high pressures, it is instead advantageous to oxidize sulfur, as it becomes the central atom in clusters of the form: N-(SH_4)-N or HN-(SH_4)-NH. This is balanced by the presence of hydrogen anions H^- while N^{3-} remains as an anion. This partial reversal in redox potential is in line with a recent computational estimation of atomic electronegativities at high pressure (at 300GPa: 5.8/10.1/6.1 for S/N/H[59] but still represents a striking reversal of chemistry. It occurs in most mixtures (except the most sulfur-rich) but only for AQS results in a

stable phase; a breakdown of enthalpy contributions shows that the resulting structure is much more compact, likely due to octahedron formation around the S^{6+} cation, which outweighs the electronic cost of ionizing the S-3p shell. In compressed H_3S, where one might consider sulfur to be octahedrally coordinated, a similar reversal of charge transfer occurs, albeit on a much smaller scale (possibly due to effective screening by the conduction electron sea).

Most stable compounds discussed here are wide-gap insulators or semiconductors. Interestingly, however, around 100GPa pressure a few compounds exhibit insulator-metal transitions. Electron-phonon coupling calculations indicate that these compounds can support electron-phonon mediated superconductivity up to about 50K. Metallization occurs due to phase transitions into inherently metallic phases and is therefore not likely to be affected by DFT's underestimation of the electronic band gap. In carbonaceous H_2S, metallization was reported already at 60 GPa[33]. It remains unusual to find "hot ice" materials that are metallic at less than very extreme temperature conditions: even above the melting line they tend to remain insulating until heated to much higher temperatures[6]. Here, we present examples of stable molecular mixtures that are metallic in the ground state and will remain so at all elevated temperature conditions.

Finally, the existence of stable hydrogen sulfide-ammonia phases beyond 100 GPa suggests that H_2S can be bound deep inside icy planets. Equation-of-state calculations suggest it might form a thin layer between ammonia hydrates and an ice-rich ocean. Its presence in this deep planetary reservoir should be considered not only for interior models but also when interpreting atmospheric measurements.

Methods

Structural predictions. Structure searches for energetically stable crystalline structures were performed on various stoichiometries of $(H_2S)_x(NH_3)_y$ from x:y=1:4 to 2:1 using simulation cells containing up to four formula units. Structure searches for all stoichiometries were carried out at 10GPa, 50GPa, and from 100GPa to 800GPa in increments of 100GPa by particle swarm optimization methodology as implemented in the CALYPSO code[60,61] and were augmented by structures drawn from the analogous $(H_2O)_x(NH_3)_y$ system[15]. The CALYPSO methodology is highly effective in finding stable or metastable structures only depending on the given chemical

composition and external conditions, and has been applied successfully to various elemental solids, binary, and ternary compounds [62-65].

Ab initio calculations. Structural optimizations and electronic structure calculations were performed in the DFT framework with the Perdew−Burke−Ernzerhof (PBE)[66] exchange-correlation functional, as implemented in the Vienna Ab initio Simulation Package code[67] The calculation of phonon-mediated superconductivity was performed with the Quantum-ESPRESSO package [68]. More detailed computational information can be found in the Supporting Information.

Phase stability calculations. Specifically, and motivated by preceding studies of the NH_3-H_2O system[45], the mixtures studied here are ammonia mono-sulfide (AMS, NH_3:H_2S = 1:1), ammonia di-sulfide (ADS, 1:2), ammonia hemi-sulfide (AHS, 2:1), ammonia tri-sulfide (ATS, 3:1), and ammonia quarter-sulfide (AQS, 4:1). The known compounds NH_4SH and $(NH_4)_2S$ fall under the AMS and AHS stoichiometries, respectively. The formation enthalpy of each H_2S-NH_3 compound is defined as $H = H[(H_2S)_x\,(NH_3)_y - xH(H_2S) - yH(NH_3)]$, where the most stable $P2_13$, and $P2_12_12_1$ phase of NH_3 and the Pbcm and P2/c phases of H_2S at the lower pressure below 60GPa were considered. When pressure increases beyond 60GPa, H_2S was identified to decompose into H_3S and S, and the formation enthalpies of H_2S-NH_3 above 60GPa were calculated relative to the most stable phases of H_3S and S [23] and NH_3 (Pma2 and $Pca2_1$)[69].

Chemical bonding analyses. Chemical bonding analyses utilized Bader's QTAIM approach[70] as implemented in the CRITIC2 code[71], the electron localization function (ELF) [72], and the Crystal Orbital Hamilton Population (COHP) analysis[73] as implemented in the LOBSTER code [74,75]. The phonon dispersion curves of stable compounds as shown in Supplementary Information are calculated at their stable pressure range [76, 77], from which it becomes clear that all of the mixtures in the H_2S-NH_3 system discussed below are dynamically stable due to the absence of imaginary phonon frequencies. Detailed information on the predicted stoichiometries/structures is presented in Supplementary Information of the Supporting Information.

AUTHOR INFORMATION

Corresponding Authors

* a.hermann@ed.ac.uk

Acknowledgements

We acknowledge funding support from the National Natural Science Foundation of China under Grant No. 11774140. L.J. Conway acknowledges studentship funding from EPSRC under grant No. EP/L015110/1. Computing resources provided by the UK national high performance computing service, ARCHER, and the UK Materials and Molecular Modelling Hub, which is partially funded by EPSRC (EP/P020194), and for which access was obtained via the UKCP consortium funded by EPSRC grant No. EP/P022561/1, are gratefully acknowledged. M.M. acknowledges the support of the National Science Foundation under Grant No. DMR-1848141

Author contributions

X.F. and A.H. designed the research; X.F., A.L. and LJ.C. performed the calculations and analyzed the data; X.F., A.H., L.J.C. and M.S. interpreted the data and contributed to the writing of the paper.

References

1. Hubbard, W.B., Nellis, W.J., Mitchell, A.C., Limaye, S.S. & McCandless, P.C. Interior structure of Neptune: comparison with Uranus. *Science* **253**, 648–651 (1991).

2. Helled, R., Anderson, J. D., Podolak, M. & Schubert, G. Interior models of Uranus and Neptune. *Astrophys. J.* **15**, 726 (2011).

3. Nettelmann, N.; Wang, K.; Fortney, J. J.; Hamel, S.; Yellamilli, S.; Bethkenhagen, M.; Redmer, R. Uranus evolution models with simple thermal boundary layers. Icarus 2016, 275, 107-116.

4. Hubbard, W. B. & Macfarlane, J. J. Structure and evolution of Uranus and Neptune. *J. Geophys. Research.* **85**, 225-234 (1980).

5. Chau, R.; Hamel, S.; Nellis, W. Chemical processes in the deep interior of Uranus. *Nat. Comm.* **2**, 203 (2001).

6. Cavazzoni, C., Chiarotti, G. L., Scandolo, S., Tosatti, E., Bernasconi, M. & Parinello, M. Superionic and Metallic States of Water and Ammonia at Giant Planet Conditions. *Science* **283**, 44-46 (1999).

7. Bethkenhagen, M., et.al. Planetary ices and the linear mixing approximation. *Astrophys. J.* **848**,

67 (2017).

8. Rauer, H. et al. The PLATO 2.0 mission. Exper Astron. **38**, 249–330 (2014).

9. Valencia, D., Guillot, T., Parmentier, V. & Freedman, R.S. Bulk composition of GJ 1214b and other sub-neptune exoplanets. *Astrophys. J.* **775**, 10 (2013).

10. Zeng, L. & Sasselov, D. The effect of temperature evolution on the interior structure of H2O-rich planets. *Astrophys J.* **784**, 96 (2014).

11. Ciprian Pruteanu, G., Ackland, G.J., Poon, W.C.K. & Loveday, J.S. When immiscible becomes miscible—Methane in water at high pressures. *Science Adv.* **3**, e1700240 (2017).

12. Liu, C. et al. Topologically frustrated ionisation in a water-ammonia ice mixture. *Nat. Commun.* **8**, 1065 (2017).

13. Kraus, D. et al. Formation of diamonds in laser-compressed hydrocarbons at planetary interior conditions. *Nat. Astron.* **1**, 606–611 (2017).

14. Bethkenhagen, M., Cebulla, D. & Redmer, R. Superionic Phases of the 1:1 Water–Ammonia Mixture. *J Phys Chem* A **119**, 10582 (2015**)** .

15. Robinson, V.N., Marqués, M., Wang, Y.C., Ma, Y.M. & Hermann, A. Novel phases in ammonia-water mixtures under pressure. *J. Chem. Phys.* **149**, 234501 (2018).

16. Conway, L.J. & Hermann, A. High Pressure Hydrocarbons Revisited: From van der Waals Compounds to Diamond. *Geosciences*, **9**, 227 (2019).

17. Liu, C., Hao, G., Wang, Y., Needs, R.J., Pickard, C.J., Sun, J., Wang, H.T. & Xing, D.X. Multiple superionic states in helium–water compounds. *Nat. Phys.* **15**, 1065–1070 (2019).

18. Song, X.Q., Yin, K.T., Wang, Y.C., Hermann, A, Liu, H.Y., Lv, J., Li, Q., Chen, C.F. & Ma, Y.M. Exotic Hydrogen Bonding in Compressed Ammonia Hydrides. *J. Phys. Chem. Lett*. **10**, 2761–2766 (2019).

19. Liu, C., Hao, G., Hermann, A., Wang, Y., Miao, M.S., Pickard, C.J., Needs, R.J., Wang, H.T., Xing, D.X. & Sun, J. Plastic and Superionic Helium Ammonia Compounds under High Pressure and High Temperature. *Phys Rev* X **10**, 021007 (2020).

20. Huang, P., Liu, H.Y., Lv, J., Li, Q., Long, C.L., Wang, Y.C., Chen, C.F., Hemley, R.J. & Ma, Y.M. Stability of H_3O at extreme conditions and implications for the magnetic fields of Uranus and Neptune. *Proc Natl Acad. Sci.* **117**, 5638-5643 (2020).

21. Grasselli, F., Stixrude, L. & Baroni, S. Heat and charge transport in H_2O at ice-giant

conditions from ab initio molecular dynamics simulations. *Nat. Commun.* **11**, 3605 (2020).

22. Duan, D., Liu, Y.X., Tian, F.B., Li, D., Huang, X.L., Zhao, Z.L., Yu, H.Y., Liu, B.B., Tian, W.J. & Cui, T. Pressure-induced metallization of dense $(H_2S)_2H_2$ with high-Tc superconductivity. *Sci Rep.* **4**, 6968 (2014).

23. Errea, I. et al. High-pressure hydrogen sulfide from first principles: A strongly anharmonic phonon-mediated superconductor. *Phys Rev Lett.* **114**, 157004 (2015).

24. Errea, I., Calandra, M., Pickard, C.J., Nelson, J., Needs, R.J., Li, Y.W., Liu, H.Y., Zhang, Y.W., Ma, Y.M. & Mauri, F. Quantum hydrogen-bond symmetrization in the superconducting hydrogen sulfide system. *Nature* **532**, 81-84 (2016).

25. Li, Y.W. et al. Dissociation products and structures of solid H_2S at strong compression. *Phys. Rev.* B, **93**, 020103(R) (2016).

26. Li, Y., Hao, J., Liu, H., Li, Y. & Ma, Y. The metallization and superconductivity of dense hydrogen sulfide. *J. Chem. Phys*. **140**, 174712 (2014).

27. Drozdov, A. P., Eremets, M. I., Troyan, I. A., Ksenofontov, V. & Shylin, S. I. Conventional superconductivity at 203 K at high pressures. *Nature* **525**, 73 (2015).

28. Pater, I.de, Romani, P.N. & Atreya, S.K. Possible microwave absorption by H_2S gas in Uranus' and Neptune's atmospheres. Icarus **91**, 220-233 (1991).

29. Irwin, P.G.J., Toledo, D., Garland, R., Teanby, N.A., Fletcher, L.N., Orton, G.A. & Bézard, B. Detection of hydrogen sulfide above the clouds in Uranus's atmosphere. Nat Astron. 2018, 2, 420-427.

30. Irwin, P.G.J., Toledo, D., Garland, R., Teanby, N.A., Fletcher, L.N., Orton, G.S. & Bezard, B. Probable detection of hydrogen sulphide (H_2S) in Neptune's atmosphere. *Icarus* **321**, 550-563 (2019).

31. Cui, W.W., Bi, T.G., Shi, J.M., Li, Y.W., Liu, H.Y.,; Zurek, E. & Hemley, R.J. Route to high-Tc superconductivity via CH_4-intercalated H_3S hydride perovskites. *Phys. Rev.* B **101**, 134504 (2020).

32. Sun, Y., Tian, Y.F., Jiang, B.W., Li, X., Li, H.F., Litaka, T., Zhong, X. & Xie, Y. Computational discovery of a dynamically stable cubic SH_3-like high-temperature superconductor at 100 GPa via CH_4 intercalation, *Phys. Rev.* B **101**, 174102 (2020).

33. Snider, E. et.al Room-temperature superconductivity in a carbonaceous sulfur hydride. *Nature* **586**, 373–377(2020).

34. Lewis, J.S. & Prinn, R.G. Jupiter's Clouds: Structure and Composition. Science **169**, 472-473 (1970).

35. Atreya, S.K., Hofstadter, M.H., In, J.H., Mousis, O., Reh, K. & Wong, M.H. Deep Atmosphere Composition, Structure, Origin, and Exploration, with Particular Focus on Critical in situ Science at the Icy Giants. *Space Sci Rev.*, **216**, 18 (2020).

36. Luszcz-Cook, S.H. & de Pater, I. Constraining the origins of Neptune's carbon monoxide abundance with CARMA millimeter-wave observations. *Icarus* **222**, 379-400 (2013).

37. Luszcz-Cook, S.H., de Pater, I. & Wright, M. Spatially-resolved millimeter-wavelength maps of Neptune. Icarus **226**, 437-454 (2013).

38. Mousis, O. et al. Scientific rationale for Uranus and Neptune in situ explorations. *Planet Space Sci.* **155**, 12-40 (2018).

39. Isambert, F. Etude de la vapeur de bisulfhydrate d'ammoniaque. *Compt. Rend.* **92**, 919-922 (1881).

40. Bragin, J., Diem, M., Guthals, D. & Chang, S. The vibrational spectrum and lattice dynamics of polycrystalline ammonium hydrosulphide. *J. Chem. Phys.* **67**, 1247-1256 (1977).

41. Ferraro, J.R., Sill, G. & Fink, U. Infrared Intensity Measurements of Cryodeposited Thin Films of NH_3, NH_4HS, H_2S, and assignments of absorption bands. *App. Spectroscopy.* **34**, 525-533 (1980).

42. Howett, J.C.A., Carlson, R.W., Irwin, P.G.J. & Calcutt, S.B. Optical constants of ammonium hydrosulfide ice and ammonia ice. *J. Opt. Soc. Am.* B **24**, 126-136 (2007).

43. Loeffler, M.J., Hudson, R.L., Chanover, N.J. & Simon, A.A. Giant-planet chemistry: Ammonium hydrosulfide (NH_4SH), its IR spectra and thermal and radiolytic stabilities. *Icarus* **258**, 181-191 (2015).

44. Loeffler, M. & Hudson, R. Coloring Jupiter's clouds: Radiolysis of ammonium hydrosulfide (NH_4SH). *Icarus* **302**, 418-425 (2018).

45. Robinson, V.N., Wang, Y.C. Ma, Y.M. & Hermann, A. Stabilization of ammonia-rich hydrate inside icy planets. *Proc. Natl. Acad. Sci.* **114**, 9003-9008 (2018).

46. Robinson, V.N. & Hermann, A. Plastic and superionic phases in ammonia–water mixtures at high pressures and temperatures. *J. Phys.: Condens. Matt.* 32, 184004 (2020).

47. Stanley, S. & Bloxham, J. Convective-region geometry as the cause of Uranus' and Neptune's

unusual magnetic fields. *Nature* **428**, 151-153 (2004).

48. Redmer, R., Mattsson, T.R., Nettelmann, N. & French, M. The phase diagram of water and the magnetic fields of Uranus and Neptune. *Icarus*, **211**, 798-803 (2011).

49. Bronstein, Y., Depondt, P., Finocchi, F. & Saitta, A.M. Quantum-driven phase transition in ice described via an efficient Langevin approach. *Phys. Rev.* B **89**, 214101 (2014).

50. Zhong, X., Hermann, A., Wang, Y.C. & Ma, Y.M. Monoclinic high-pressure polymorph of AlOOH predicted from first principles. *Phys. Rev.* B **94**, 224110 (2016).

51. Hermann, A. High-pressure phase transitions in rubidium and caesium hydroxides. *Phys. Chem. Chem. Phys.* **18**, 16527-16534 (2016).

52. Berthold, H.J., Preibsch, W. & Vonholdt, E. On the Structure of the Cation $N_2H_7^{\oplus}$ with an N-H···N Hydrogen Bond in the Monoammonia Adduct of Ammonium Iodide. *Angew. Chem. Int. Ed.* **27**, 1524-1525 (1988).

53. Irsen, S.H., Jacobs, P. & Dronskowski, R. Tetrasulphur tetranitride: Phase transition and crystal structure at elevated temperature. *Zeitschrift fuer Anorganische und Allgemeine Chemie* **627**, 321-325 (2001).

54. Zaghoo, M., Salamat, A. & Silvera, I.F. Evidence of a first-order phase transition to metallic hydrogen. *Phys. Rev.* B. **93**, 155128 (2016).

55. McWilliams, R.S., Dalton, D.A., Mahmood, M.F. & Goncharov, A.F. Optical Properties of Fluid Hydrogen at the Transition to a Conducting State. *Phys. Rev. Lett.* **116**, 255501 (2016).

56. Endo, S., Honda, A., Koto, K., Shimomura, O., Kikegawa, T. & Hamaya, N. Crystal structure of high-pressure phase-IV solid hydrogen sulfide. *Phys. Rev.* B **57**, 5699 (1998).

57. Li, Y.W. et al. Dissociation products and structures of solid H2S at strong compression. *Phys. Rev.* B **93**, 020103(R) (2016).

58. Mcmillan, W.L. Transition temperature of strong-coupled superconductors. *Phys. Rev.* 167, 331 (1968).

59. Rahm, M. & Hoffmann, R. Squeezing All Elements in the Periodic Table: Electron Configuration and Electronegativity of the Atoms under Compression. *J. Am. Chem. Soc.* **141**, 10253–10271 (2019).

60. Wang, Y., Lv, J., Zhu, L. & Ma, Y. Crystal structure prediction via particle-swarm optimization. *Phys. Rev.* B **82**, 94116 (2010).

61. Wang, Y., Lv, J., Zhu, L. & Ma, Y. CALYPSO: A method for crystal structure prediction. *Comput. Phys. Commun.* **183**, 2063-2070 (2012).

62. Lv, J., Wang, Y., Zhu, L. & Ma, Y. M. Predicted Novel High-Pressure Phases of Lithium. *Phys. Rev. Lett.* **106**, 015503 (2011).

63. Li, X.F. & Peng, F. Superconductivity of pressure-stabilized vanadium hydrides. *Inorg. Chem.* **56**, 13759-13756 (2017).

64. Peng, F., Sun, Y., Pickard, J.P., Needs, R.J., Wu, Q. & Ma, Y.M. Hydrogen clathrate structures in rare earth hydrides at high pressures: possible route to room-temperature superconductivity. *Phys. Rev. Lett.* **119**, 107001 (2017).

65. Li, X.F., Liu, H.Y. & Peng, F. Crystal structures and superconductivity of technetium hydrides under pressure. *Phys. Chem. Chem. Phys.* 19, 28791-28796 (2016).

66. Perdew, J.P., Burke, K. & Ernzerhof, M. Generalized gradient approximation made simple. *Phys. Rev. Lett.* **77**, 3865 (1996).

67. Kresse, G.; Furthmüller, J. Efficient iterative schemes for ab initio total-energy calculations using a plane-wave basis set. Phys. Rev. B 1996, 54, 11169.

68. Giannozzi, P., Baroni, S., Bonini, N., Calandra, M., Car, R., Cavazzoni, C., Ceresoli, D., Chiarotti, G.L., Cococcioni, M. & Dabo, I. Quantum Espresso: a modular and open-source software project for quantum simulations of materials. *J. Phys.: Condens. Matt.* **21**, 395502 (2009).

69. Pickard, C.J. & Needs, R. J. Highly compressed ammonia forms an ionic crystal. *Nat. Mat.* **7**, 775-779 (2008).

70. Bader, R. F. W. Atoms in Molecules: A Quantum Theory. (Clarendon: Oxford, UK, 1990).

71. Otero-de-la-Roza, A., Johnson, E.R. & Luaña, V. Critic2: A program for real-space analysis of quantum chemical interactions in solids. *Comput. Phys. Comm.* **185**, 1007-1018 (2014).

72. Becke, A.D. & Edgecombe, K.E. A simple measure of electron localization in atomic and molecular systems. *J. Chem. Phys.* **92**, 5397-5403 (1990).

73. Dronskowski, R. & Blöchl, P.E. Crystal orbital hamilton populations (COHP): Energy-resolved visualization of chemical bonding in solids based on density-functional calculations. *J. Phys. Chem.* **97**, 8617-8624 (1993).

74. Maintz, S., Deringer, V.L., Tchougréeff, A.L. & Dronskowski, R. Analytic projection from

plane-wave and PAW wave functions and application to chemical-bonding analysis in solids. *J Comput. Chem.* **34**, 2557-2567 (2013).

75. Maintz, S., Deringer, V.L., Tchougréeff, A.L. & Dronskowski, R. LOBSTER: A tool to extract chemical bonding from plane-wave based DFT. J. Comput. Chem. **37**, 1030-1035 (2016).

76. Togo, A., Oba, F. & Tanaka, I. First-principles calculations of the ferroelastic transition between rutile-type and $CaCl_2$-type SiO_2 at high pressures. *Phys. Rev.* B **78**, 134106 (2008).

77. Togo, A. & Tanaka, I. First principles phonon calculations in materials science. *Scr. Mater.* **108**, 1-5 (2015).

Figures and Tables

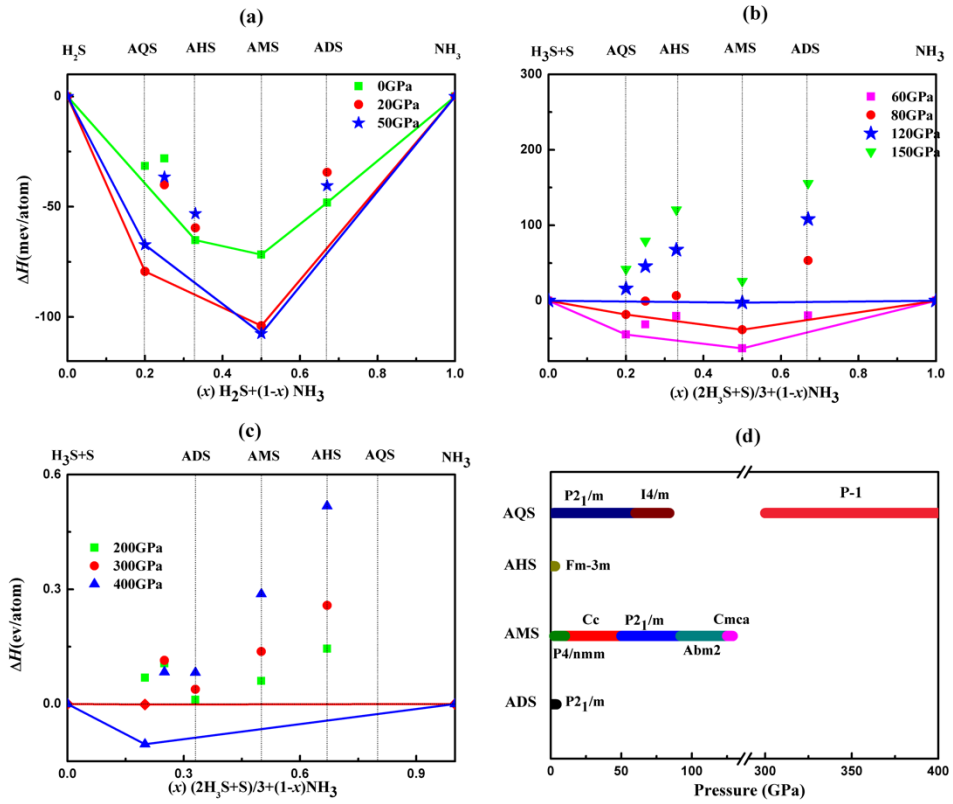

Figure 1 Convex hulls of the H_2S-NH_3 system relative to (a) H_2S and NH_3, (b) (c) H_3S+S and NH_3, and (d) ground state phase diagram under pressure.

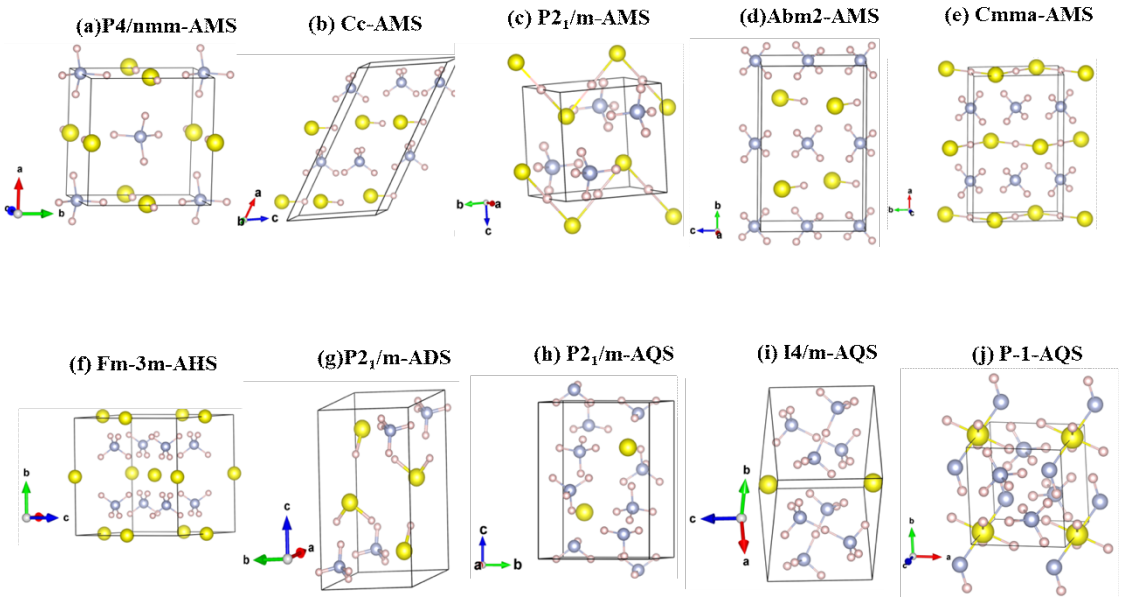

Figure 2 The crystal structures of stable compounds in the H_2S-NH_3 system. Yellow (blue, pink) spheres denote sulfur (nitrogen, hydrogen) atoms, and covalent bonds are indicated by thin lines.

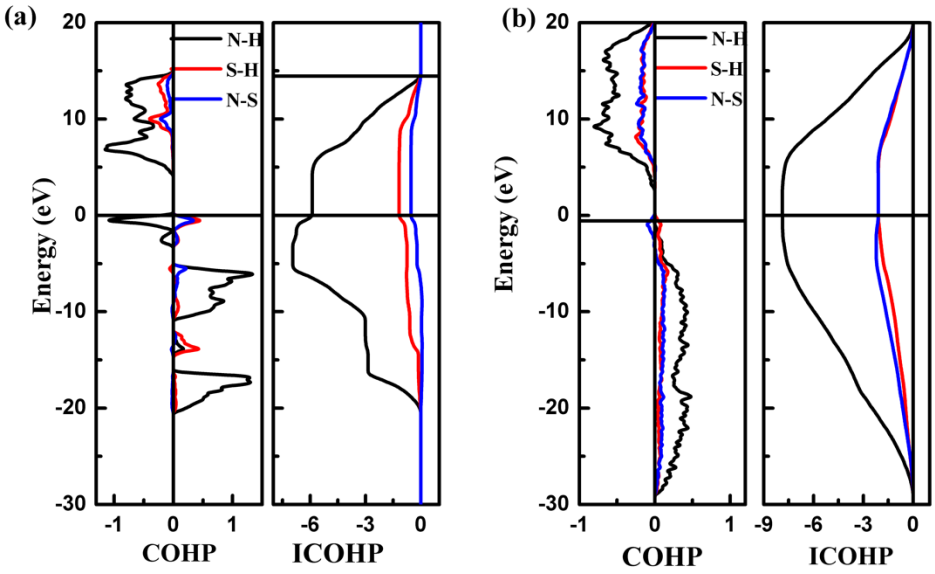

Figure 3 The COHP and ICOHP of AQS phases under pressure. (a) I4/m-AQS at 70 GPa, (b) P-1-AQS at 400 GPa.

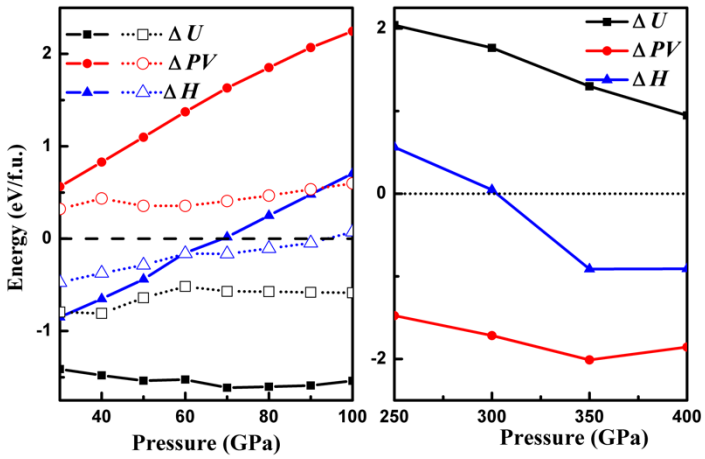

Figure 4 Calculated ΔH, ΔU, and $\Delta(PV)$ for AQS phases as a function of pressure. (a) $P2_1/m$ (solid lines) and I4/m (dotted lines). (b) P-1-AQS. Both graphs are relative to the decomposition $4NH_3 + (2H_3S+S)/3$.

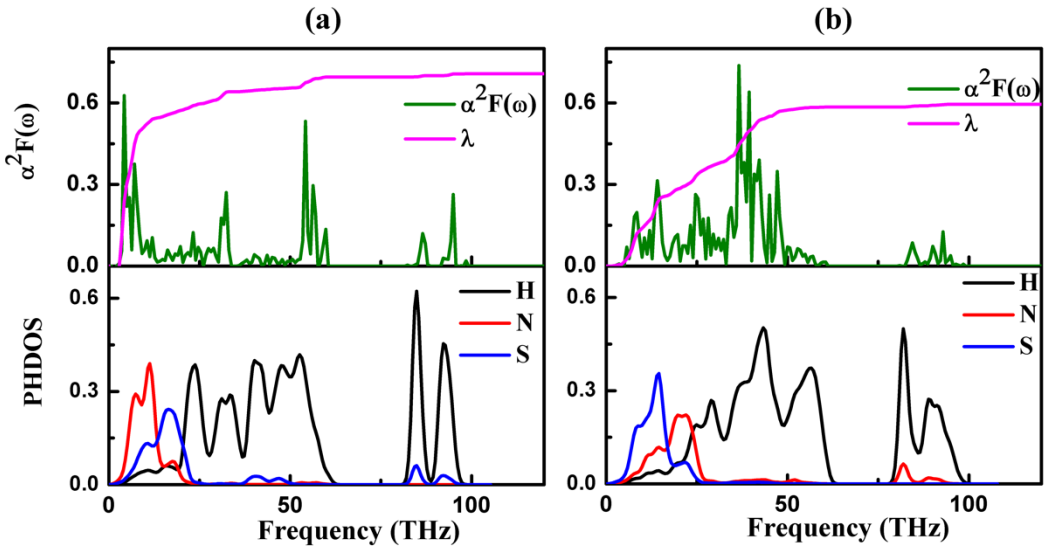

Figure 5 Eliashberg spectral function $\alpha^2F(\omega)$ and integrated electron phonon coupling parameter λ (top) and projected phonon densities of state (PHDOS, bottom) for (a) Abm2-AMS at 100GPa, (b) Cmma-AMS at 200GPa.

Table 1 Calculated EPC Parameter (λ), Logarithmic Average Phonon Frequency (ω_{log}) and superconducting temperature (T_c) for stable phases of AMS at the pressures given.

Phase	Pressure	λ	ω_{log} (K)	T_c (K)
Abm2	100GPa	0.703	398	13.9
	120GPa	0.772	493	21.4
Cmma	150GPa	0.995	697	49.9
	200GPa	0.625	987	27.9